Numerical simulation for all-optical Thomson scattering X-ray source*

Tan Fang(谭 放)[a)b)], Zhu Bin(朱 斌)[a)], Han Dan(韩 丹)[a)], Xin Jian-Ting(辛建婷)[a)], Zhao Zong-Qing(赵宗清)[a)], Cao Lei-Feng(曹磊峰)[a)], Gu Yu-Qiu(谷渝秋)[a)†], and Zhang Bao-Han(张保汉)[a)]

[a)] *Science and Technology on Plasma Physics Laboratory, China Academy of Engineering Physics, Mianyang* 621900, *China*
[b)] *Department of Modern Physics, University of Science and Technology of China, Hefei* 230026, *China*

(Received 23 June 2013; revised manuscript received 19 August 2013; published online 20 February 2014)

Energy spectra, angular distributions, and temporal profiles of the photons produced by an all-optical Thomson scattering X-ray source are explored through numerical simulations based on the parameters of the SILEX-I laser system (800 nm, 30 fs, 300 TW) and the previous wakefield acceleration experimental results. The simulation results show that X-ray pulses with a duration of 30 fs and an emission angle of 50 mrad can be produced from such a source. Using the optimized electron parameters, X-ray pulses with better directivity and narrower energy spectra can be obtained. Besides the electron parameters, the laser parameters such as the wavelength, pulse duration, and spot size also affect the X-ray yield, the angular distribution, and the maximum photon energy, except the X-ray pulse duration which is slightly changed for the case of ultrafast laser–electron interaction.

Keywords: ultrashort laser, wakefield acceleration, Thomson scattering, X-ray source

PACS: 41.75.Jv, 52.38.Kd, 52.38.Ph, 52.59.Px **DOI:** 10.1088/1674-1056/23/3/034104

1. Introduction

The generation of bright, ultrafast, and tunable hard X-rays through tabletop systems has been pursued by a number of groups worldwide.[1] This novel X-ray source would have a wide variety of applications, such as atomic and molecular motion studies on the femtosecond time scale, advanced biomedical imaging, and lossless detection of high Z materials.[2–4] Among many different ultrafast X-ray sources, e.g., free-electron lasers (FEL),[5] laser-driven K_α sources,[6] and high harmonic generation sources (HHG),[7] the Thomson scattering source,[8,9] which is produced by the scattering of the laser photons on a relativistic electron beam, possesses a set of valuable characteristics, including compactness, tunable photon energy, potential for a duration of the femtosecond scale, and high brightness. The method has already been demonstrated through picosecond and femtosecond lasers synchronized to a linear accelerator (linac)[10–12] with a peak brightness as high as 10^{20} photons/mm^2/mrad^2/s/0.1%. This kind of new sources are also established in Tsinghua University and Shanghai Institute of Applied Physics.[13,14]

Compared with the conventional Thomson scattering source, an improved source known as the all-optical Thomson scattering X-ray source was proposed by Catravas and Esarey in 2001,[15] in which the electrons are produced through the laser wakefield acceleration in plasma. The electron wakefield acceleration method was proposed in 1979[16] and has been anticipated to have the potential of producing quasi-monoenergetic electron beams with low divergence, small energy spread, and ultrashort pulse duration (less than 10 fs).[17–19] The electron beams with such novel qualities can be applied to the Thomson scattering X-ray source, which has been studied theoretically.[15] Successful experimental demonstrations of the laser wakefield acceleration were achieved by three groups[20–22] in 2004, and then in 2006[23] with better stability and reproducibility. The following experimental results of all-optical Thomson scattering sources have been obtained with photon energy ranging from 400 eV to 2 keV,[24] which shows the feasibility to produce a compact ultrashort X-ray source with low divergence, small energy spread, and high brightness. In 2012, the newest experiment applied a novel design in which a plasma mirror was combined with the laser-wakefield accelerator, and X-rays with energy of hundreds of keV were produced.[25] That design deeply reduces the difficulty of laser–electron temporal and spatial synchronization, becoming the most promising way for the all-optical Thomson scattering source now.

2. Model and method

2.1. Theoretical model

In 1906, the first Thomson scattering phenomenon was discovered by Thomson,[26] in which the photons acquire blueshifts through scattering off the relativistic electrons. From the field point of view, the electrons will gain quiver

*Project supported by the National Natural Science Foundation of China (Grant Nos. 10902010 and 10975121), the Foundation of China Academy of Engineering Physics (CAEP) (Grant No. 2009A0102003), and the Foundation of Laboratory of Science and Technology on Plasma Physics, RCLF, CAEP (Grant No. 9140C680305120C68252).

†Corresponding author. E-mail: YQGu@caep.ac.cn

© 2014 Chinese Physical Society and IOP Publishing Ltd

motion perpendicularly to their initial motion direction in the laser electromagnetic field. Such motion produces a figure of eight in the reference frame that moves together with the electrons.[27]

To identify the influence of the electron quiver motion and the laser intensity on the Thomson scattering process, the normalized laser vector potential is defined as[28]

$$a_0 = \frac{v_{\rm os}}{c} = \frac{eA_{\rm L}}{mc^2} = 0.85\times 10^{-9}\lambda\sqrt{I}, \tag{1}$$

where $v_{\rm os}$ is the oscillation velocity of the electron quiver motion, e and m are the electron charge and mass, respectively, c is the velocity of light, $A_{\rm L}$ is the amplitude of the laser vector potential, λ is the laser wavelength in units of μm, and I is the laser intensity in units of 10^{18} W/cm^2.

For the case of $a_0 \ll 1$, the electron quiver motion is far less than the axial motion. The corresponding source is identified as in the linear Thomson regime. When a_0 approaches or exceeds unity, the electron quiver motion velocity approaches the speed of light. The corresponding source is identified as in the nonlinear Thomson regime.

In the linear Thomson regime, the angular frequency of the scattered photons is[10]

$$\omega_x = \omega_0\frac{2\gamma^2(1-\cos\alpha)}{1+\gamma^2\theta^2}, \tag{2}$$

where ω_x and ω_0 are the angular frequencies of the scattered and the laser photons, respectively, γ is the normalized energy of the electrons defined as $\gamma = W/mc^2$, α is the collision angle, and θ is the scattering angle. The differential cross section of the photons scattered by the electrons is[29]

$$\frac{{\rm d}\Sigma}{{\rm d}\Omega} = \left(\frac{e^2}{mc^2}\right)^2\frac{1}{\gamma^2(1-\beta\cos\theta)^2} \times\left(1-\frac{\sin^2\theta\cos^2\phi}{\gamma^2(1-\beta\cos\theta)^2}\right), \tag{3}$$

where θ and ϕ are the spatial angles. According to Eq. (3), the differential cross section has a maximum at $\theta = 0$ and the scattered photons mainly emit within a cone with a solid angle of $1/\gamma$. The $1/\gamma$ will decrease with the increase of the electron energy, so the scattered photons will have a narrower angular distribution for higher electron energy.

At a higher laser intensity, for the nonlinear Thomson scattering, the electron quiver motion velocity approaches the speed of light, which has attracted many theoretical[28,30–35] and experimental[36–39] studies. In the nonlinear Thomson regime, the angular frequency of the scattered photons is[31]

$$\omega_n = \frac{2}{2+a_0^2}\gamma^2(1-\beta_{z0})^2 n\omega_0, \tag{4}$$

where $n = 1,2,3,\ldots$, and β_{z0} is the electron initial axial velocity. According to Eq. (4), in the nonlinear regime, one electron can absorb n photons with angle frequency ω_0 and emit one photon with angle frequency ω_n,[27] which can be understand from the quantum mechanics point of view. Meanwhile, as a nonlinear effect, the $\omega_1 = \frac{2}{2+a_0^2}\gamma^2(1-\beta_{z0})^2\omega_0$ term will decrease with the increase of the laser intensity a_0.

The duration of the scattered X-ray pulse is related to the pulse duration and the spot sizes of both the electron and the laser beams[29,40]

$$\sigma_{\rm T} = \frac{\sigma_{\rm ez}\sqrt{(1-\cos\alpha)(\sigma_{\rm ex}^2+\sigma_{\rm lx}^2)+(1+\cos\alpha)\sigma_{\rm lz}^2}}{c\sqrt{(1-\cos\alpha)(\sigma_{\rm ex}^2+\sigma_{\rm lx}^2)+(1+\cos\alpha)(\sigma_{\rm ez}^2+\sigma_{\rm lz}^2)}} = \begin{cases} \sigma_{\rm ez}/c, & \alpha = 180^\circ, \\ \dfrac{\sigma_{\rm ez}\sqrt{\sigma_{\rm ex}^2+\sigma_{\rm lx}^2+\sigma_{\rm lz}^2}}{c\sqrt{\sigma_{\rm ex}^2+\sigma_{\rm ez}^2+\sigma_{\rm lx}^2+\sigma_{\rm lz}^2}}, & \alpha = 90^\circ, \end{cases} \tag{5}$$

where $\sigma_{\rm ez}$, $\sigma_{\rm ex}$ are the bunch length and the spot size of the electron beam, respectively, and $\sigma_{\rm lz}$, $\sigma_{\rm lx}$ are those of the laser beam. For $\alpha = 180^\circ$, the duration of the scattered X-ray pulse is completely determined by the electron bunch length. For $\alpha = 90^\circ$, the duration of the scattered X-ray pulse is related to the bunch length and the beam spot sizes of both the electron and the laser beams. For the case of all-optical Thomson scattering, the bunch length of the wakefield accelerated electron beam is as short as the driven laser bunch length, which leads to the main dependence on the electron bunch length of the scattered X-ray pulse duration.

2.2. Numerical simulation

CAIN is a Fortran Monte–Carlo code for the numerical simulation of the interaction involving high energy electrons, positrons, and photons, which starts with the name ABEL. The first version of CAIN is a combined program of modified ABEL and a laser QED code.[41] In our study, the newest version, CAIN2.35, is applied,[42] which can handle the physics processes such as the interaction of high energy photon or electron/positron including the nonlinear effects of the field strength. This code is still used by many groups.[11,39] In our simulation, the electron beams are divided into 50000 macro particles and the electrons in every macro particle share the same parameters. The electron spins are ignored and the parameter n in Eq. (4) has a maximum value of 5. The spatial, energy, and temporal parameters of both electrons and laser photons obey the Gaussian distribution.

Through simulations with the same electron and laser experimental parameters reported in Refs. [43] and [44] using CAIN, the calculated magnitude of the photon yield is equal to that of the corresponding experimental results, which ensures the effectiveness of this code.

3. Results and analysis

In this section, we present our simulation results based on the laser parameters of system SILEX-I at China Academy of Engineering Physics (CAEP) and the previous experimental results of laser wakefield electron acceleration. We also study the optimizations of electron and laser parameters and the influence of the laser parameters. For simplification, the laser and the electron beams are perfectly matched.

In the previous experiments,[45] the SILEX-I system produced a laser beam with a total energy of 2.1 J, 20% energy in the focal spot, a wavelength of 800 nm, a pulse duration of 30 fs, and a spot size of 26 μm. The wakefield accelerated electrons had novel parameters, such as an energy of 58 MeV, an energy spread of 15 %, charge of 0.34 nC, and emittance of 0.3 mm·mrad. The electron beam spot size and bunch length are chosen to be 20 μm and 30 fs, respectively. In our source design, the laser beam is divided into two beams which contain 90% and 10% of the total energy respectively. The beam with 90% energy accelerates the electrons to several tens of MeV through the wakefield acceleration, while the other beam is scattered off the accelerated electrons, producing X-ray photons with an energy of several tens of keV. The simulated photon angular distribution and the energy spectra are shown in Fig. 1.

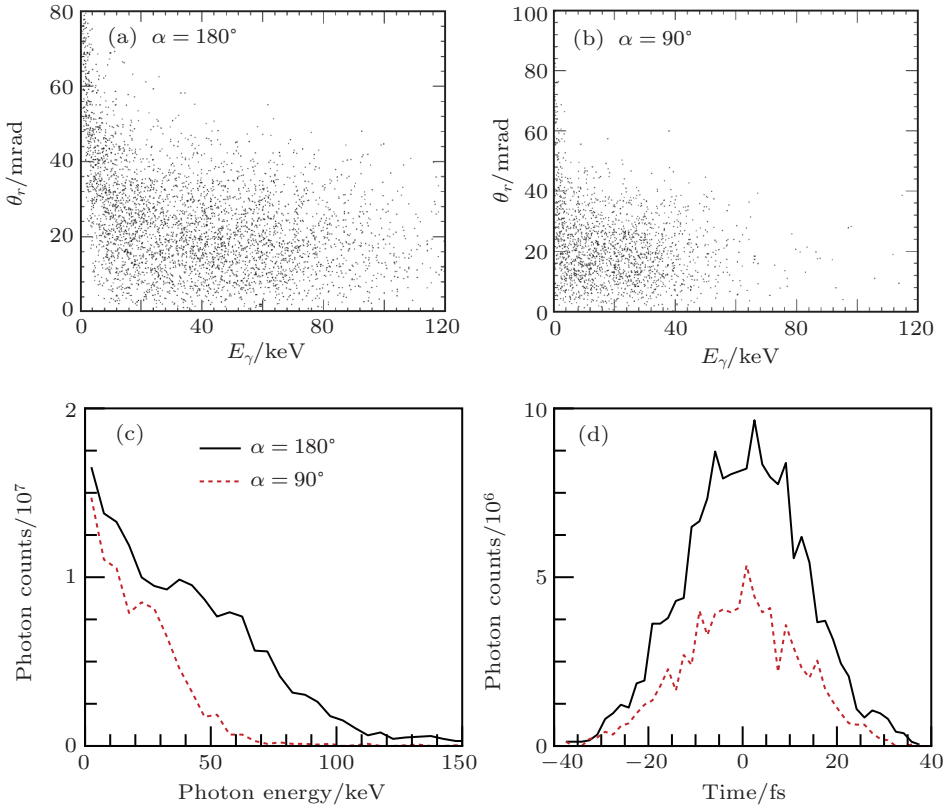


Fig. 1. (color online) Simulation results for the laser parameters and the laser wakefield electron acceleration results on the SILEX-I system. (a) The photon angular distribution produced through 180° Thomson scattering; (b) the photon angular distribution produced through 90° Thomson scattering; (c) the energy spectra for the scattered photons; (d) the temporal profile for the scattered photons.

From Figs. 1(a) and 1(b), we can see that for the electron parameters above, the scattered photons will emit with a large energy spread from 0 keV to 120 keV and an angle distributing from 0 mrad to 50 mrad. Such a wide distribution results from the broad energy spread and the large emittance of the electrons. The photon energy spectra in Fig. 1(c) shows that a higher total photon yield and more high energy photons can be produced for $\alpha = 180°$, while a narrower energy spectrum can be obtained for $\alpha = 90°$.

In both 180° and 90° cases, photons with several tens of keV energy can be obtained. However practically, the time and spatial synchronizations are more difficult to fulfill for $\alpha = 90°$, which results in the reduction of the photon yield. In Fig. 1(d), the temporal profile of the scattered photons shows that the X-ray pulse duration remains nearly unchanged for both cases, which is coincident with the results of Eq. (5) under the ultrashort laser–electron interaction case.

From Fig. 1, it can be concluded that, with such param-

eters, the photon emittance and energy spread are too large to limit the practical application. To overcome this shortcoming, the electron beam parameters are optimized to reduce the photon emittance according to our previous study on the electron parameters.[46] The optimized results are shown in Fig. 2. Compared with Fig. 1, the scattered photons shown in Figs. 2(a) and 2(b) emit within a smaller angular range of 20 mrad. It is also clear that for a certain scattering angle, the photons distribute in two regions with different energies corresponding to $n = 1$ and 2 in Eq. (4), where the upper region possesses nearly twice the energy of the other. For the optimized electron parameters, the energy spectrum in Fig. 2(c) shows peaks around 70 keV for $\alpha = 180°$ and around 30 keV for $\alpha = 90°$, which may be applied as a monochromatic X-ray source.

The X-ray pulse parameters deeply depend on both the electron and the laser parameters. The contributions of the electron parameters have been analyzed in our previous work,[46] so for the purpose of a further investigation, the simulation results for different laser parameters are presented here in Figs. 3–5. For concision, only the cases with $\alpha = 180°$ are presented here.

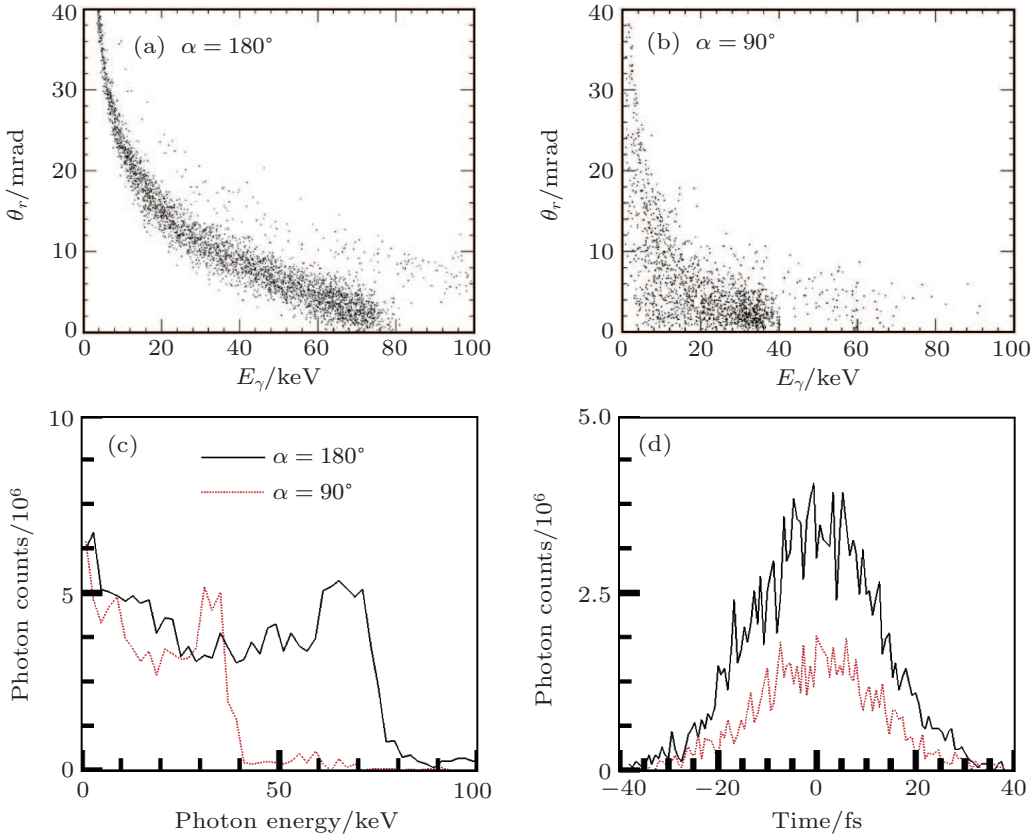


Fig. 2. (color online) Simulation results for optimized laser and electron parameters. The electron energy spread and emittance are reduced to 2% and 0.03 mm·mrad, respectively. To gain a higher yield, the laser intensity is shifted to 2.169×10^{18} W/cm^2, corresponding to $a_0 = 1$. Other parameters are the same as those in Fig. 1. Panels (a)–(d) show the corresponding figures of Fig. 1.

At first, the simulation results for different laser wavelengths are presented in Fig. 3. For a certain laser system, it is reasonable to fix its pulse energy to a certain value in the simulation, so the different wavelength will lead to different a_0 (seeing Eq. (1)) and ω_0. As a result of a lower a_0, the suppression of the nonlinear Thomson scattering and the increase of the scattered photon energy can be obtained for a shorter laser wavelength. From Figs. 3(a)–3(c), the nonlinear scattered photons corresponding to $n = 2$ vanish gradually and the maximum photon energy extends from 40 keV to 80 keV.

Then let us consider the simulation results for different laser pulse durations shown in Fig. 4. Similar to Fig. 3, for a fixed pulse energy, different pulse duration will lead to different a_0, also resulting in the suppression of the nonlinear Thomson scattering and a similar photon angular distribution. But in Figs. 4(a) and 4(b), the photon energy obtains a slightly blueshift with the increase of the pulse duration, which can be explained as the contribution of the decreased a_0^2 term in the denominator of Eq. (4). For a longer laser duration in Fig. 4(c), the photon angular distribution is nearly the same as that in Fig. 4(b) because of the total vanishing of the nonlinear effects.

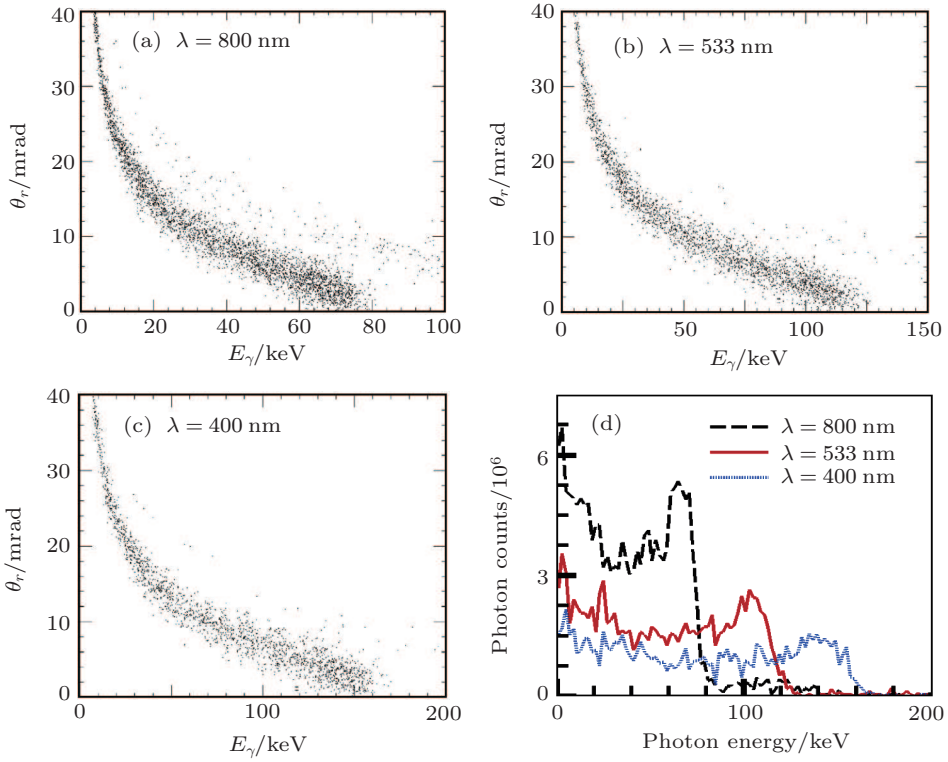


Fig. 3. (color online) (a)–(c) Photon angular distributions for different laser wavelengths and (d) the energy spectra for the optimized laser and electron parameters similar to Fig. 2. Three laser wavelengths (800 nm, 533 nm, 400 nm) are used.

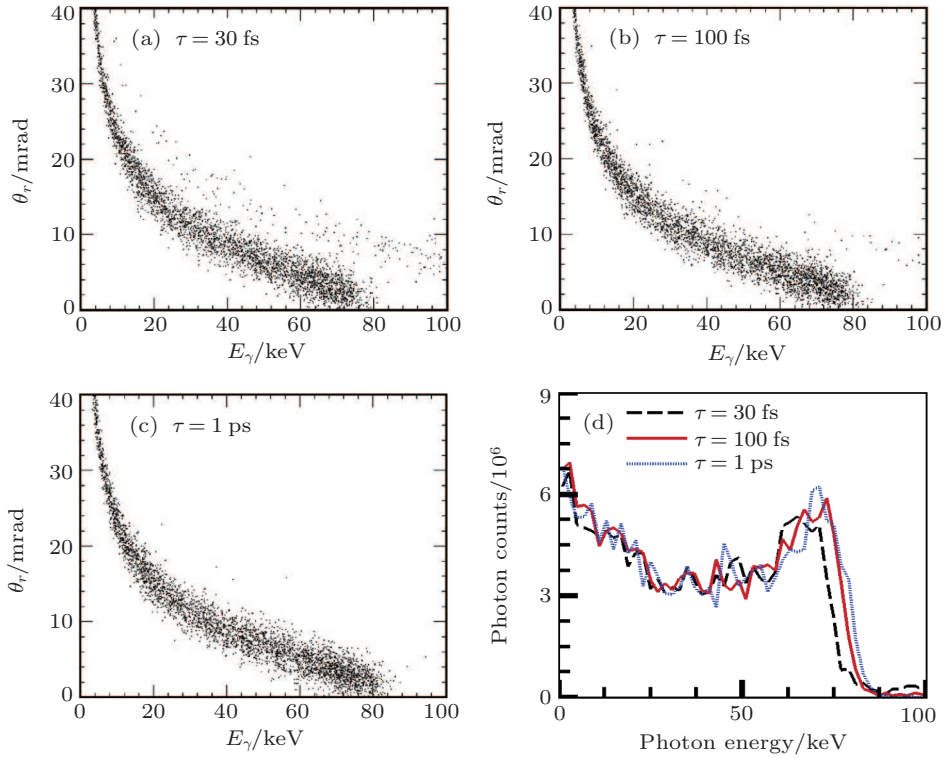


Fig. 4. (color online) (a)–(c) Photon angular distributions for different laser pulse durations and (d) the energy spectra. The parameters are the same as those in Fig. 3, except the laser wavelength is 800 nm and the laser duration is increased from 30 fs to 1 ps.

When the laser is focused into different spot sizes, the corresponding laser intensity, initial photon emittance, and interaction region are different, leading to more complex results as shown in Fig. 5. The laser far-field emission angle θ_{laser} is related to its waist ω_{laser}

$$\theta_{\text{laser}} = \frac{\lambda}{\pi \omega_{\text{laser}} \eta}, \tag{6}$$

where λ is the laser wavelength and η is the refractive index.

Usually the laser spot size is equal to its waist. In Fig. 5(a), the laser spot size is a small value of 5 μm, leading to a small interaction region, a high laser intensity, and a large collision angle α. In such case, the nonlinear Thomson scattering cannot be ignored, leading to several regions with different energies for a certain angle. Furthermore, for electrons with a certain emission angle, the large collision angle α will lead to scattered photons with a wide angular distribution and a large energy spread. It can be seen more clearly from the dotted line in Fig. 5(d) that the energy spectrum for $\sigma = 5$ μm is similar to a negative exponential distribution and the peak structure around tens of keV disappears. For a larger spot size, e.g., $\sigma = 40$ μm in Fig. 5(c), the scattered photons distribute with narrower angle and energy spread, with a visible peak around 35 keV. However the disadvantage of the larger spot size is that the total photon yield is lower than that in the small spot case. So a moderate laser spot size is needed to balance the photon yield and the angular distribution. Under our simulation parameters, $\sigma = 26$ μm is a suitable laser spot size.

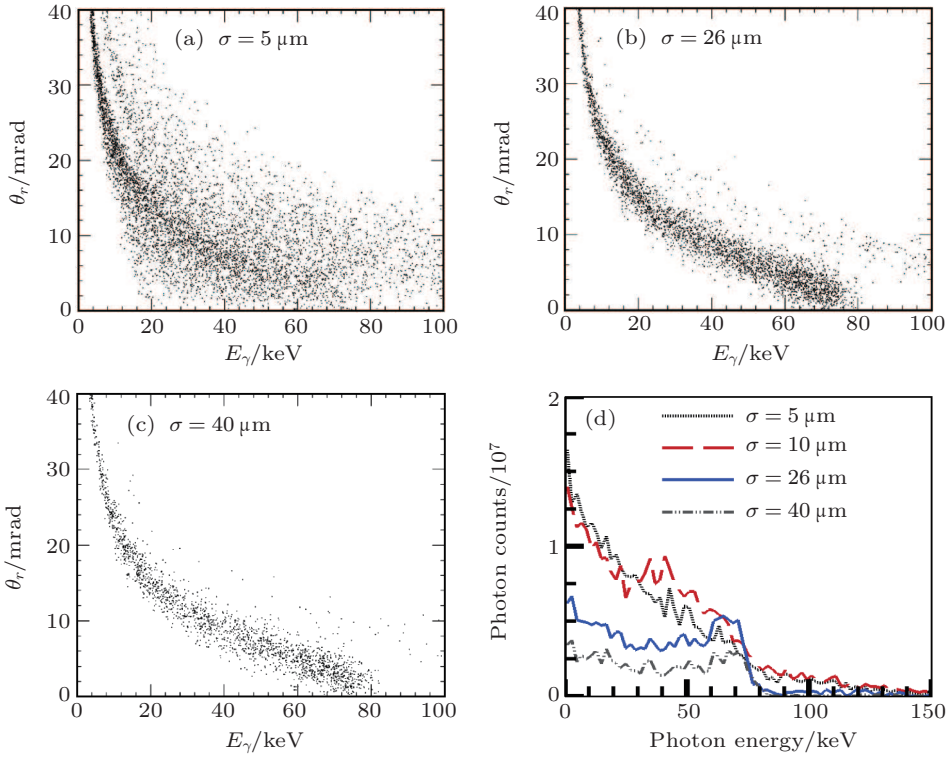


Fig. 5. (color online) (a)–(c) Photon angular distributions for different laser spot sizes and (d) the energy spectra. The parameters are the same as those in Fig. 3, except the laser wavelength is 800 nm and the laser waist is altered from 5 μm to 40 μm.

4. Conclusion and outlook

In summary, for the purpose of obtaining an optimized all-optical Thomson scattering source, we have studied the energy spectra, angular distributions, and time profiles of the scattered photons produced by an all-optical Thomson scattering X-ray source through numerical simulations based on the parameters of the SILEX-I system and the previous experiment results of laser wakefield electron acceleration on that system. The numerical simulations show that X-ray pulses with a duration of tens of femtoseconds can be produced. But for the electrons with a large emittance and a wide energy spread, the scattered photons possess a wide angular distribution and a large energy spread. Optimizations are made based on such results and our previous studies for different electron parameters. Using the optimized electron parameters, X-ray photons with a narrower angular distribution and a smaller energy spread can be obtained.

Furthermore, the influences of the laser parameters are also studied, which show the suppression of the nonlinear Thomson scattering with the increases of the laser frequency, the pulse length, and the spot size. A larger laser spot size will lead to X-ray pulses with a smaller angular distribution, a narrower energy spread, and a visible peak in the spectrum, but the total photon yield is lower than that in the small spot case. So under our simulation parameters, $\sigma = 26$ μm is a suitable laser spot size.

Only the angular distribution, energy spectra, and time profiles of the scattered photons for different laser and electron parameters are presented here. The simulation results and theoretical explanation for the photon yield and brightness under

different interaction angles and different laser–electron time delays will be conducted in our future work.

References

[1] Wei X F, Huang X, Peng H, Wang X, Zeng X, Zhou K, Guo Y, Liu L, Wang X, Zhu Q and Lin D 2008 *J. Phys.: Conf. Ser.* **112** 032010

[2] Joshi C J and Corkum P B 1995 *Phys. Today* **48** 36

[3] Schoenlein R W, Leemans W P, Chin A H, Volfbeyn P, Glover T E, Balling P, Zolotorev M, Kim K J, Chattopadhyay S and Shank C V 1996 *Science* **274** 236

[4] Attwood D 1999 *Soft X-rays and Extreme Ultraviolet Radiation: Principles and Applications* (Cambridge: Cambridge University Press)

[5] Arthur J, Materlik G, Tatchyn R and Winick H 1995 *Rev. Sci. Instrum.* **66** 1987

[6] Rousse A, Rischel C and Gauthier J C 2001 *Rev. Mod. Phys.* **73** 17

[7] Bartels R, Backus S, Zeek E, Misoguti L, Vdovin G, Christov I P, Murnane M M and Kapteyn H C 2000 *Nature* **406** 164

[8] Sprangle P, Ting A, Esarey E and Fisher A 1992 *J. Appl. Phys.* **72** 5032

[9] Sprangle P and Esarey E 1992 *Phys. Fluids B* **4** 2241

[10] Gibson D J, Anderson S G, Barty C P J, Betts S M, Booth R, Brown W J, Crane J K, Cross R R, Fittinghoff D N, Hartemann F V, Kuba J, Sage G P L, Slaughter D R, Tremaine A M, Wootton A J, Hartouni E P and Springer P T 2004 *Phys. Plasmas* **11** 2857

[11] Pogorelsky I V, Ben-Zvi I, Hirose T, Kashiwagi S, Yakimenko V, Kusche K, Siddons P, Skaritka J, Kumita T, Tsunemi A, Omori T, Urakawa T, Washio M, Yokoya K, Okugi T, Liu Y, He P and Chine D 2000 *Phys. Rev. ST Accel. Beams* **3** 090702

[12] Leemans W P, Schoenlein R W, Volfbeyn P, CHin A H, Glover T E, Balling P, Zolotorev M, Kim K J, Chattopadhyay S and Shank C V 1996 *Phys. Rev. Lett.* **77** 4182

[13] Tang C X, Huang W H, Li R K, Du Y C, Yan L K, Shi J R, Du Q, Yu P C, Chen H B, Du T B, Cheng C and Lin Y Z 2009 *Nucl. Instr. Meth. A* **608** S70

[14] Luo W, Xu W, Pan Q Y, Fan G T, Li Y J, Liu G Q, Xu B J, Xu Y, Yan Z and Yang L F 2009 *Proc. SPIE* **7385** 73852D

[15] Catravas P, Esarey E and Leemans W P 2001 *Meas. Sci. Technol.* **12** 1828

[16] Tajima T and Dawson J M 1979 *Phys. Rev. Lett.* **43** 267

[17] Esarey E, Hubbard R F, Leemans W P, Ting A and Sprangle P 1997 *Phys. Rev. Lett.* **79** 2682

[18] Esarey E, Schroeder C B and Leemans W P 1999 *Phys. Plasmas* **6** 2262

[19] Umstadter D, Kim J K and Dodd E 1996 *Phys. Rev. Lett.* **76** 2073

[20] Faure J, Glinec Y, Pukhov A, Kiselev S, Gordienko S, Lefebvre E, Rousseau J P, Burgy F and Malka V 2004 *Nature* **431** 541

[21] Mangles S P D, Murphy C D, Najmudin Z, Thomas A G R, Collier J L, Dangor A E, Divall E J, Foster P S, Gallacher J G, Hooker C J, Jaroszynski D A, Langley A J, Mori W B, Norreys P A, Tsung F S, Viskup R, Walton B R and Krushelnick K 2004 *Nature* **431** 535

[22] Geddes C G R, Toth Cs, Tilborg J V, Esary E, Schroeder C B, Bruhwiler D, Nieter C, Cary J and Leemans W P 2004 *Nature* **431** 538

[23] Faure J, Rechatin C, Norlin A, Lifschitz A, Glinec Y and Malka V 2006 *Nature* **444** 737

[24] Schwoerer H, Liesfeld B, Schlenvoigt H P, Amthor K U and Sauerbrey R 2006 *Phys. Rev. Lett.* **96** 014802

[25] Phuoc K T, Corde S, Thaury C, Malka V, Tafzi A, Goddet J P and Shah R C 2012 *Nature Photon.* **6** 308

[26] Thomson J J 1906 *Conduction of Electricity through Gases* (Cambridge: Cambridge University Press)

[27] Gibbon P 2005 *Short Pulse Laser Interactions with Matter* (London: Imperial College Press) p. 50

[28] Ride S K, Esarey E and Baine M 1995 *Phys. Rev. E* **52** 5425

[29] Huang W H, He X Z, Huang G, Tang C X and Lin Y Z 2004 *High Energy Physics and Nuclear Physics* **28** 446 (in Chinese)

[30] Esarey E, Ride S K and Sprangle P 1993 *Phys. Rev. E* **48** 3003

[31] Lau Y Y, He F, Umstadter D P and Kowalczyk R 2003 *Phys. Plasmas* **10** 2155

[32] Li D, Yokoya K, Hirose T and Hamatsu R 2003 *Jpn. J. Appl. Phys.* **42** 5376

[33] Ugaz E 1994 *Phys. Rev. A* **50** 34

[34] Lan P F, Lu P X and Cao Wei 2007 *Acta Phys. Sin.* **56** 2482 (in Chinese)

[35] Zhang P, Song Y R and Zhang Z G 2006 *Acta Phys. Sin.* **55** 6208 (in Chinese)

[36] Englert T J and Rinehart E A 1983 *Phys. Rev. A* **28** 1539

[37] Chen S Y, Maksimchuk A and Umstadter D 1998 *Nature* **396** 653

[38] Bula C, McDonald K T, Prebys E J, Bamber C, Boege S, Kotseroglou T, Melissinos A C, Meyerhofer D D, Ragg W, Burke D L, Field R C, Horton-Smith G, Odian A C, Spencer J E, Walz D, Berridge S C, Bugg W M, Shmakov K and Weidemann A W 1996 *Phys. Rev. Lett.* **76** 3116

[39] Babzien M, Ben-Zvi I, Kusche K, Pavlishin I V, Pogorelsky I V, Siddons D P, Yakimenko V, Cline D, Zhou F, Hirose T, Kamiya Y, Kumita T, Omori T, Urakawa J and Yokoya K 2006 *Phys. Rev. Lett.* **96** 054802

[40] Kim J, Chattopadhyay S and Shank C V 1994 *Nuc. Inst. Meth. Phys. Res. A* **341** 351

[41] Chen P, Horton-Smith G, Ohgaki T, Weidemann A W and Yokoya K 1995 *Nucl. Instr. Meth. A* **335** 107

[42] Yokoya K 2003 *User's Manual of CAIN*. version 2.35

[43] Anderson S G, Barty C P J, Betts S M, Brown W J, Crane J K, Cross R R, Fittinghoff D N, Gibson D J, Hartemann F V, Kuba J, LeSage G P, Rosenzweig J B, Slaughter D R, Springer P T and Tremaine A M 2004 *Appl. Phys. B* **78** 891

[44] Albert F, Anderson S G, Gibson D J, Hagmann C A, Johnson M S, Messerly M, Semenov V, Shverdin M Y, Rusnak B, Tremaine A M, Hartemann F V, Siders C W, McNabb D P and Barty C P J 2010 *Phys. Rev. ST Accel. Beams* **13** 070704

[45] Dong K G, Gu Y Q, Zhu B, Wu Y C, Cao L F, He Y L, Liu H J, Hong W, Zhou W M, Zhao Z Q, Jiao C Y, Zhang B H and Wang X F 2010 *Acta Phys. Sin.* **59** 8733 (in Chinese)

[46] Tan F, Zhu B, Zhao Z Q, Cao L F, Gu Y Q and Zhang B H 2011 *High Power Laser and Partical Beams* **23** 1233